Journal of Computational Electronics
https://doi.org/10.1007/s10825-019-01317-3

Theoretical investigation of the structural, electronic and thermodynamic properties of cubic and orthorhombic $XZrS_3$ (X = Ba,Sr,Ca) compounds

Mouloud Oumertem[1] · D. Maouche[2] · Saadi Berri[2,3] · N. Bouarissa[3] · D. P. Rai[4] · R. Khenata[5] · M. Ibrir[3]

Abstract
The structural, electronic and thermodynamic properties of $XZrS_3$ (X = Ba,Sr,Ca) compounds with orthorhombic *Pbnm* and cubic *Pm-3m* phases have been investigated and reported. The calculations have been performed using various density functionals within the generalized gradient approximation. The obtained lattice parameters for the *Pnma* phase reveal very good agreement with experiment. The computed electronic band structures show that in the cubic phase the material of interest is an indirect band-gap (*R–Γ*) semiconductor, whereas it is a direct band gap (*Γ–Γ*) in the orthorhombic phase. The semiconducting $XZrS_3$ (X = Ba,Sr,Ca) compounds are found to satisfy the stability criteria against volume change. Based on the quasi-harmonic Debye model, the thermodynamic properties of the material in question have been predicted taking into account the lattice vibrations. The variation of the lattice constant, bulk modulus, heat capacity, Debye temperature and thermal expansion coefficient as a function of pressure in the range 0–30 GPa and temperatures of 0–1500 K has been computed. Our findings show that external effects such as temperature and pressure are highly effective in tuning some of the macroscopic properties of the compounds under study.

Keywords Chalcogenide perovskite · Phase stability · Electronic properties · Thermodynamic properties · Ab initio calculations

1 Introduction

Due to their possible applications in many industrial and engineering domains [1–6], perovskites with different compositions and structures have attracted much attention. These materials have many interesting properties, such as mixed conducting oxides for gas separation [7], metallicity and insulating [8], high-temperature electrodes [9], cathode [10], photo-electrode and photo-catalytic [11], photodetector [12], photovoltaic [13], solid electrolyte [14]), hydrogen sensor [15–17], piezoelectric transducer [18], thermostat actuator [19], dielectric resonator [20], magnetic memory and ferromagnetism [21–23], electro-optical modulator [24, 25], laser [26, 27], superconductor [28–30], semiconductivity [31] and ferroelectricity [32, 33].

Recently, perovskite compounds like $CeMnO_3$, Rb(Mn,V, Co, Fe)F_3 and $BaNpO_3$ have been reported to be a half-metallic ferromagnet [34–36]. Similar results were also reported for various other compounds, such as $CuMn_2InSe_4$ [37], Li_6XCl_8 (X = V, Mn, Co and Fe) Suzuki-type compounds [38], (Cr, Mn and V)-doped SrO [39, 40], Sr_2GdReO_6 double perovskite [41] and quaternary Heusler compound FeCrRuSi [42].

As opposed to their oxide and halide siblings, polycrystalline chalcogenide perovskites ($BaZrS_3$, $CaZrS_3$ and $SrZrS_3$) have received a little attention. Therefore, only limited data have been published on their physical properties. These

✉ Saadi Berri
berrisaadi12@yahoo.fr

1 Department of Physics, Faculty of Sciences, University of Setif 1, Sétif, Algeria

2 Laboratory for Developing New Materials and Their Characterizations, University of Setif 1, Sétif, Algeria

3 Department of Physics Faculty of Science, University of Mohamed Boudiaf, M'Sila, Algeria

4 Department of Physics, Pachhunga University College, Aizawl 796001, India

5 Laboratoire de Physique Quantique et de Modélisation Mathématique (LPQ3M), Département deTechnologie, Université de Mascara, 29000 Mascara, Algeria

Published online: 01 March 2019

materials have proven to be very useful for solar energy conversion applications [43–47]. Their strongly ionic character makes them provide a new avenue for engineering the semiconducting properties for applications, such as energy harvesting, solid-state lighting and sensing.

It should be mentioned that the electronic structure and dielectric constants of $BaZrS_3$ and $CaZrS_3$ compounds have been investigated by Sun et al. [48] in three different phases using first-principle calculations. Moreover, Hong et al. [49] have studied the alloy system $BaZr_{1-x}Ti_xS_3$ suggesting the tunability of the energy band gap. More recently, the electronic band structure of $BaZrS_3$, $SrZrS_3$ and $CaZrS_3$ in the *Pbnm* phase has been studied by Kuhar et al. [50] using projector augmented wave (PAW) formalism as implemented in the GPAW code [51] and reported band-gap energy values of 2.25, 2.5 and 2.48 eV for $BaZrS_3$, $SrZrS_3$ and $CaZrS_3$, respectively.

In Sect. 4 of this paper, the structural, electronic and thermodynamic properties of $XZrS_3$ are presented. The aim of this work is to examine the electronic band structure of the perovskite $XZrS_3$, with emphasis on its derived properties. The calculations are performed with a full relativistic version of the full-potential augmented plane wave (FP–LAPW) and the pseudopotential plane wave (PP–PW) methods within Perdew-Burke-Ernzerhof (PBE)-GGA, Engel-Vosko (EV)–GGA, Hubbard U term GGA + U, Wu and Cohen (WC)-GGA and GGA-Sol as exchange correlation potentials. The remainder of the paper is organized as follows: The theoretical background is described in Sect. 2. Results are presented and discussed in Sect. 3. A summary of the results is given in Sect. 4.

2 Computational methods

In the present work, the experimental crystal structure as reported by Lelieveld and Ijdo [52] has been considered. XZrS3 compounds crystallize in the orthorhombic (space group *Pnma*) structure which is similar to the black structure of $CsSnI_3$ and cubic symmetry (space group *Pm3m*). The crystal structures of $XZrS_3$ compound are illustrated in Fig. 1.

The present computations are performed through the FP-LAPW method using DFT as implemented in WIEN2 K code [53]. In the study of structural properties, the exchange correlation energy is treated within the GGA as parameterized by the PBE-GGA method [54]. As a matter of fact, the use of the Engel–Vosko (EV) [55] and Hubbard parameter (GGA + U) [56] approaches so as to treat the exchange–correlation potential is very efficient for studying strongly correlated electrons where the energy band gap of the material of interest can be evaluated more accurately. In these cases, the core electrons are taken to be relativistic, whereas the

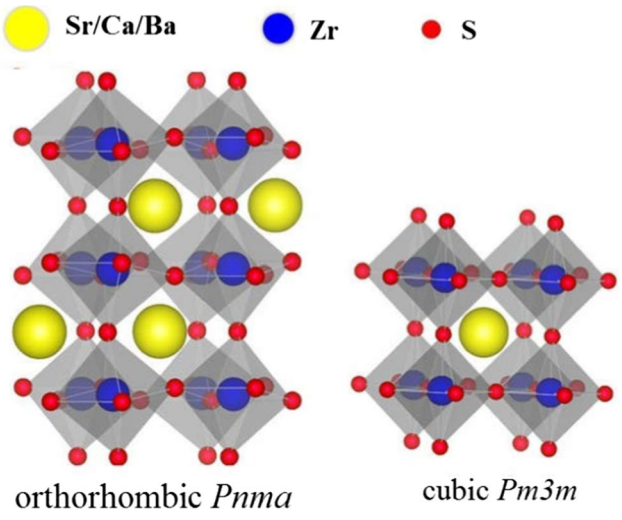

Fig. 1 Crystal structure of orthorhombic *Pbnm* and cubic *Pm-3m* phases of $XZrS_3$ compounds

valence electrons are considered to be as semi-relativistic. This is probably best suited for our system and for a full-potential method. The threshold energy between valence and core states is set to be -6.0 Ry. Here, the Kohn–Sham equations are solved by expanding the wave functions in the spherical harmonics form inside the atom spheres. A plane wave expansion has been used in the interstitial regions of atoms inside the unit cell. We have used $l\max = 10$ for angular momentum expansion and $R_{MT}K_{max} = 8$ as a plane wave cutoff with 500 and 3000 k points for orthorhombic and cubic phases, respectively. Here, R_{MT} is the average muffin-tin (MT) radius and K_{max} is the wave function cutoff. The radii R_{MT} of the muffin tins (MT) are chosen to be approximately proportional to the corresponding ionic radii. The energy between successive iterations is converged to 0.0001 Ry, and forces are minimized to 1 mRy $Bohr^{-1}$.

We have also used the ultra-soft pseudo-potentials of the Vanderbilt-type [57], and the GGA approach according to PBE [54], GGA-Sol [58] and GGA-WC [59] was already used to calculate structural and electronic properties of $XZrS_3$. A computer program CASTEP (Cambridge Serial Total Energy Package) [60] was already used to calculate structural and electronic properties of $XZrS_3$. The kinetic cutoff energy for the plane wave expansion is taken to be 500 eV for all cases being considered here. The special k point sampling for the integration of first Brillouin zone has been employed by using the Monkhorst–Pack method with $10 \times 10 \times 10$ k points for a cubic phase and $7 \times 7 \times 7$ k points for the orthorhombic phase. Based on the Broyden–Fletcher–Goldfarb–Shanno (BFGS) [61] minimization technique, the system reached the ground state via self-consistent calculation when the total energy is stable to within 5×10^{-6} eV $atom^{-1}$ the force is less than 10^{-2} eV $Å^{-1}$.

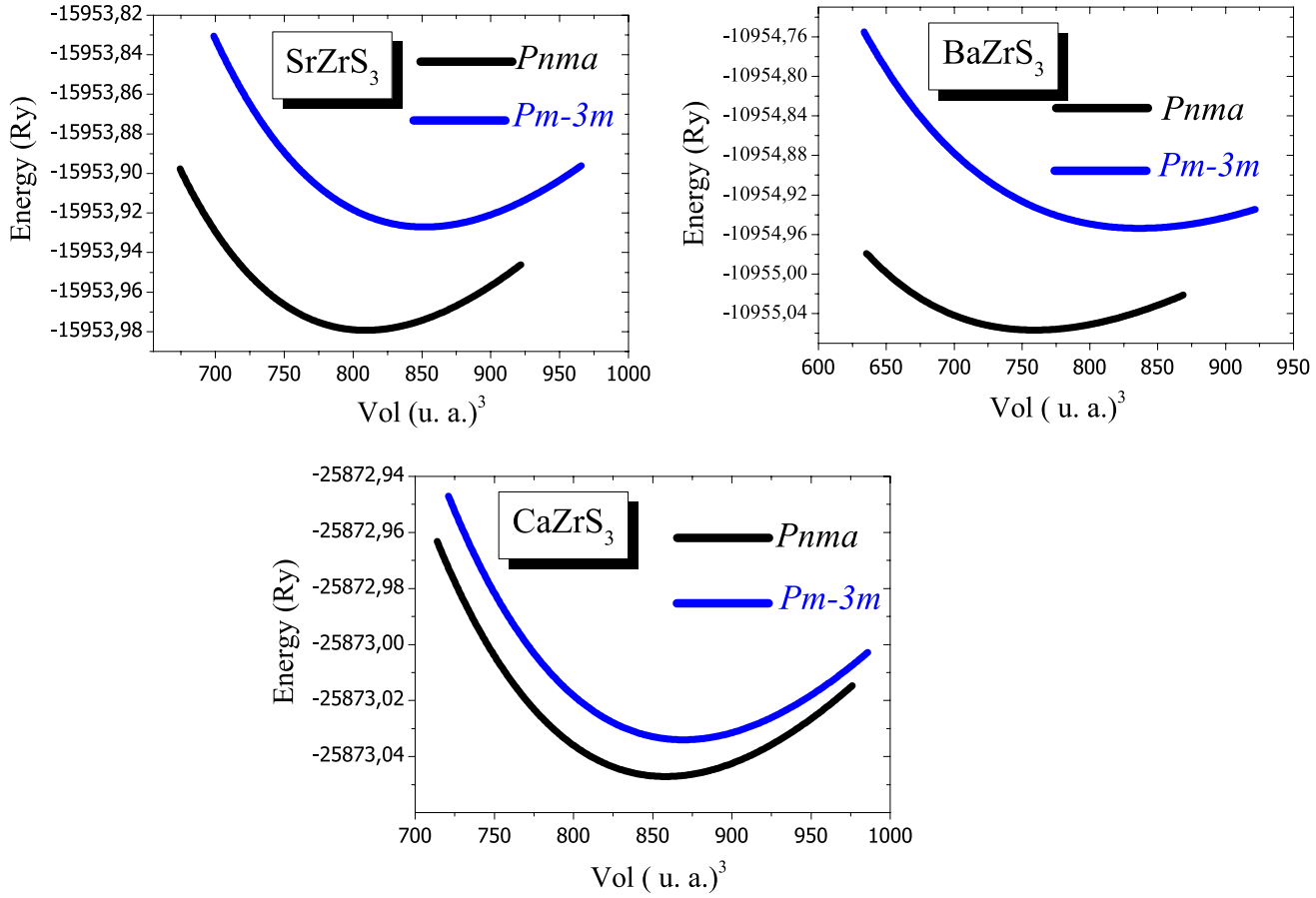

Fig. 2 Calculated normalized energy as a function of volume for $XZrS_3$ compound

To investigate the thermodynamic properties of $XZrS_3$ compounds, the quasi-harmonic Debye model [62] has been applied. In this model, the non-equilibrium Gibbs function $G^*(V;P,T)$ is expressed as follows:

$$G^*(V;P,T) = E(V) + PV + AVib[\theta(V);T] \quad (1)$$

where $E(V)$ is the total energy per unit cell, PV corresponds to the constant hydrostatic pressure condition, $\theta(V)$ is the Debye temperature and $Avib$ is a vibrational term that can be written using the Debye model of the phonon density of states as [63],

$$A_{\text{vib}}(\theta;T) = nkT\left[\frac{9\theta}{8T} + 3\ln(1 - e^{-\theta/T}) - D(\theta/T)\right] \quad (2)$$

where n is the number of atoms per formula unit and $D(\theta/T)$ is the Debye integral. For an isotropic solid, θ is given as [64],

$$\theta_D = \hbar\left[6\pi^2 V^{1/2} n\right]^{1/3} f(\rho)\sqrt{\frac{B_S}{Mk_B^2}} \quad (3)$$

where M is the molecular mass per unit cell and B_S is the adiabatic bulk modulus. The latter is approximated by the static compressibility [63] as

$$B_S \cong B(V) = V\frac{\mathrm{d}^2E(V)}{\mathrm{d}V^2} \quad (4)$$

$f(\rho)$ in Eq. (3) is reported in Refs. [64, 65]. The Poisson ratio ν is taken to be 0.25 [66]. Thus, the non-equilibrium Gibbs function $G^*(V;P,T)$ versus (V; P, T) is minimized with respect to the volume V as

$$\left[\frac{\partial G^*(V;P,T)}{\partial V}\right]_{P,T} = 0 \quad (5)$$

By solving Eq. (5), one can obtain the thermal equation of state (EOS) $V(P,T)$. The heat capacity C_V and the thermal expansion coefficient α are given by [67, 68],

$$C_V = 3nk\left[4D\left(\frac{\theta}{T}\right) - \frac{3\theta/T}{e^{\theta/T} - 1}\right] \quad (6)$$

Table 1 Lattice constant a (Å), b (Å), c (Å), bulk modulus B (in GPa) and first pressure derivative of bulk modulus B' for $XZrS_3$

Compound		a	b	c	V_0	B	B'
$BaZrS_3$							
Pnma	FP-LAPW	7.0598	9.9813	7.0250	495.0235	73.2240	4.1562
	PP-PW	7.1753	10.0570	7.0534	508.9873	123.4053	–
	Exp [52]	7.0599	9.9813	7.0251	495.04	–	–
	[70]	7.04	9.98	7.05	–	–	–
	Other [77]	7.054	7.155	10.068	–	–	–
	[77]	7.112	7.299	10.181	–	–	–
	[78]	7.06	7.16	10.04	–	–	–
	[78]	7.03	7.12	10.00	–	–	–
Pm-3m	FP-LAPW	5.0504	–	–	126,5060	72.5519	4.1477
	PP-PW	5.0211	–	–	128.3901	69.3380	
	Exp [70]	4.192	–	–	–	–	–
	Other [78]	4.195	–	–	–	–	–
	[73]	4.242	–	–	–	–	–
	[75]	4.198	–	–	–	–	–
	[77]	4.234	–	–	–	–	–
	[77]	4.207	–	–	–	150	–
$CaZrS_3$							
Pnma	FP-LAPW	7.0856	9.6647	6.5588	449.1479	82.4513	4.1716
	PP-PW	7.0719	9.6611	6.5817	449.6771	105.7320	–
	Exp [52]	7.0300	9.5896	6.5366	440.66		
Pm-3m	FP-LAPW	4.9859	–	–	123.9455	75.3506	3.7145
	PP-PW	4.9801	–	–	123,5059	74.4015	
	Exp [79]	4.020	–	–	–	–	–
	Exp [81]	4.138		–	–	–	–
	Other [82]	4.064	177.7	–	–	–	–
$SrZrS_3$							
Pnma	FP-LAPW	7.1474	9.8425	6.8046	478.6919	77.3524	4.1462
	PP-PW	7.1692	9.8362	6.7839	478.3849	101.9356	–
	Exp [52]	7.1085	9.7661	6.7350	467.56	–	–
	Other [78]	6.79	7.16	9.84	–	–	–
	[78]	6.75	7.13	9.79	–	–	–
Pm-3m	FP-LAPW	5.0163	–	–	126,2265	73.4956	3.9978
	PP-PW	5.0085	–	–	125.6385	71.1959	

$$S = nk\left[4D\left(\frac{\theta}{T}\right) - 3\ln(1 - e^{-\theta/T})\right] \tag{7}$$

$$\alpha = \frac{\gamma C_V}{B_T V} \tag{8}$$

where γ is the Grűneisen parameter, which is defined as

$$\gamma = -\frac{\mathrm{d}\ln\theta(V)}{\mathrm{d}\ln V} \tag{9}$$

Through the quasi-harmonic Debye model, one could calculate the thermodynamic quantities at any given temperatures and pressures of $XZrS_3$ compounds from the obtained E–V data at $T=0$ and $P=0$.

3 Results and discussion

The total energy has been obtained versus the unit-cell volume V_0 for both orthorhombic (*Pnma*) and cubic (*Pm-3m*) phases of the material system of interest. Our results are displayed in Fig. 2 and fit to the Murnaghan equation of state [69]. This allowed the determination of the equilibrium lattice constants a (Å), b (Å) and c (Å) and bulk modulus B (GPa) and its first pressure derivative B'. The resulting structural parameters for both phases being considered in the present work are listed in Table 1. Also shown for comparison are the available experimental and theoretical data quoted in the literature. A good accord can be observed between our findings and the experimental [52, 70, 71, 79, 80] and previous theoretical data [72–78, 81] regarding a

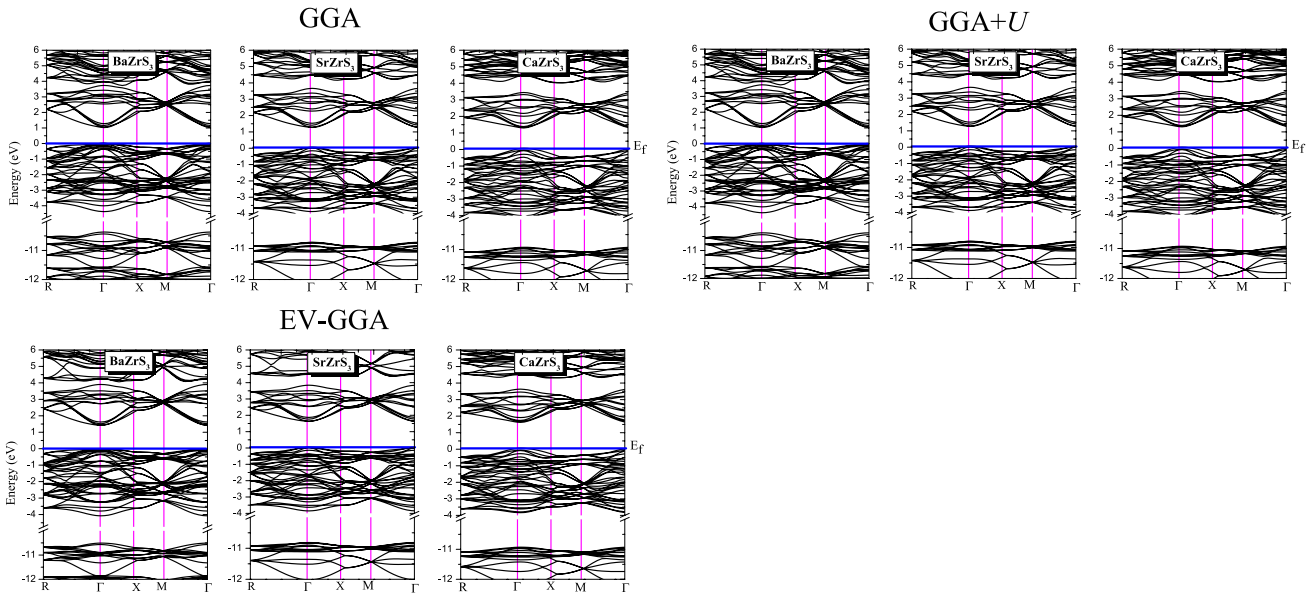

Fig. 3 Band structure for high-symmetry directions in the Brillouin zone of orthorhombic *Pbnm* structure

(Å), *b* (Å) and *c* (Å) lattice parameters. Our results indicate that the *Pnma* phase of $XZrS_3$ is at its ground state. It can also be seen that V_0 for both orthorhombic (*Pnma*) and cubic (Pm-3m) phases has an increasing trend along the sequence Ca → Sr → Ba. The increase in V_0 for X = Ca, Sr and Ba successively satisfies the increasing order of the X atomic radii, namely r(Ca = 1.64 Å) < r(Sr = 1.72 Å) < r(Ba = 1.88 Å) [82]. The behavior seems to be similar to that of $RbMF_3$ (M = Be, Mg, Ca, Sr and Ba) compounds [83]. As shown in Table 1, our results regarding the bulk modulus B of $BaZrS_3$ in the cubic (Pm-3m) phase yielded a value of 72.55 GPa when using FP-LAPW method and a value of 69.34 GPa when using PP-PW method. As compared to the value of B = 150 GPa reported by Bilić and Gale [76], our results seem to be much smaller than those of Ref. [76]. The disagreement between our results and those of Bilić and Gale [76] may be attributed to the neglect of the barium $5s^2$ and $5p^6$ electrons in the valence configuration of Ba. B is a measure of the material crystal rigidity. Thus, as far as the value of B is large, the material becomes more rigid. In our case, B increases in the following order: $B(KAlO_3) > B(RbAlO_3) > B(CsAlO_3)$. The increasing trend reveals that the rigidity and the hardness of the material in question increase in the same sequence.

Figures 3 and 4 show, respectively, the self-consistent scalar relativistic band structures and density of states of $XZrS_3$ in its both orthorhombic and cubic phases. The band structure and density of states computed via the FP–LAPW approach are shown as a prototype given the fact that the band profiles obtained from FP–LAPW approach are quite similar to those calculated via PP-PW method with a negligible difference in details. Based on the lattice symmetry, the integration paths *R–Γ–X–M–Γ* are performed so as to treat the band structure for both phases of interest, i.e., orthorhombic and cubic phases. For the orthorhombic phase, both the valence band maximum (VBM) and the conduction band minimum (CBM) occur at the high-symmetry point *Γ* in the Brillouin zone. Hence, in this phase the material being studied here is a direct band-gap semiconductor. However, as far as the cubic phase is concerned, the VBM occurs at R point and the CBM is located at the *Γ* point. Therefore, the material in question is an indirect band-gap semiconductor in its cubic phase. The computed energy band gaps given in Table 2 for the orthorhombic phases seem to be underestimated with respect to the experimental ones of 1.8 [76, 80], 2.13 [76] and 1.9 eV [76] reported for $BaZrS_3$, $SrZrS_3$ and $CaZrS_3$, respectively. The previous computational studies appear to give much larger values than those found in the present work for most cases of interest. It is worth noting that the computed energy band gaps of all compounds being studied here are calculated better (as compared to experiment) when using the GGA-EV approximation. The disagreement of our results with respect to experiment is due to the use of GGA approach which is well known to underestimate the energy band gaps with respect to experiment.

The nature of the electronic band structure has been elucidated by calculating the total and partial densities of states (DOS) of $BaZrS_3$, $SrZrS_3$ and $CaZrS_3$ compounds in the energy range − 12 to 6 eV (see Fig. 5). By observing Fig. 5,

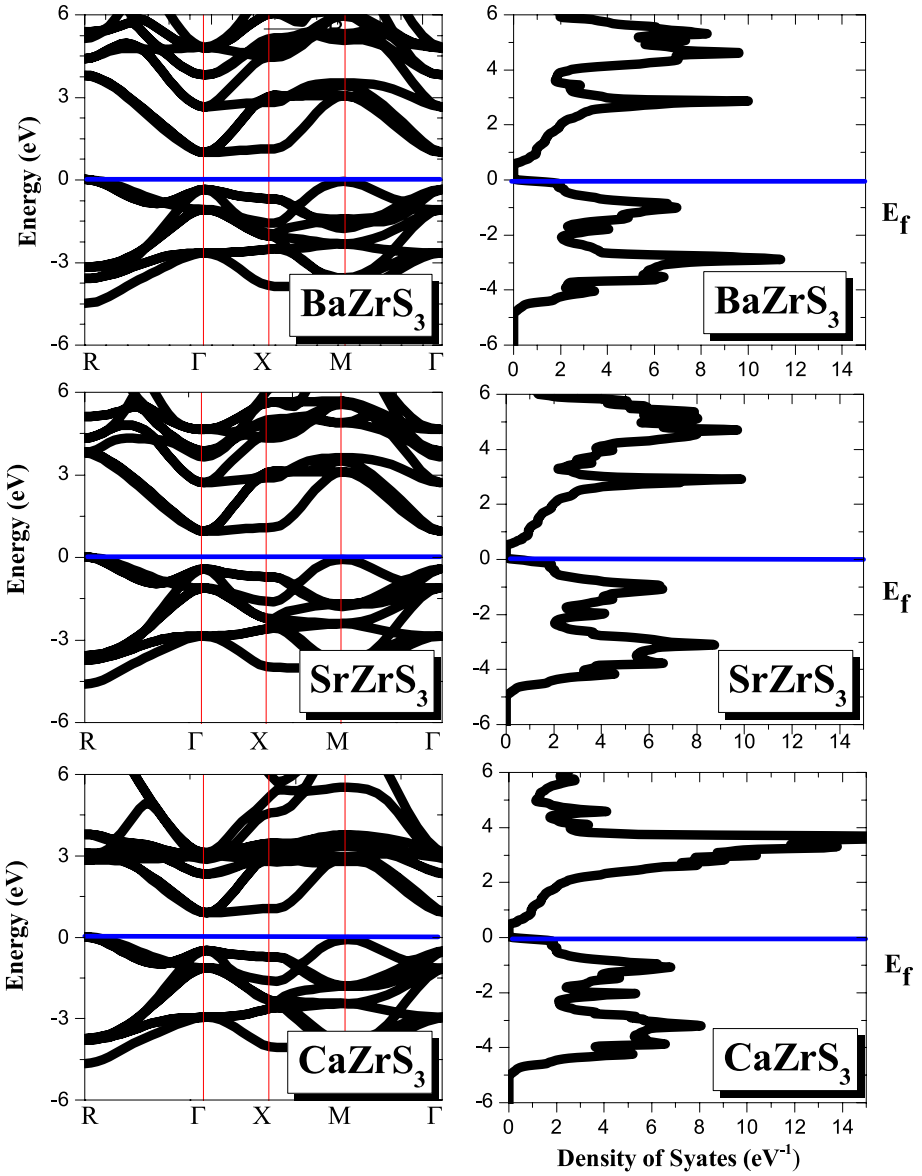

Fig. 4 Band structure and total density of states of cubic *Pm-3m* structure using PBE-GGA method

one can note that the overall features of the DOS for all compounds of interest are similar. At low energies and in particular in the core states the main contribution is due to the hybridization of X–p and S–s states. Nevertheless, the valence bands are considered in the energy range from −4 to 0.0 eV. In the valence band, mixed S–p and X–p states are prominent. The conduction band is above the Fermi level. This band is essentially composed of X–s and Zr–d states. Meanwhile, the electronic structure has also been computed versus pressure and is plotted in Fig. 6. We observe a clear shift of the Fermi level. Nevertheless, one can note a preserved semiconducting nature for both band structures of interest in the stress range of 0% up to 14%.

The thermodynamic properties of the compounds of interest have also been investigated under high pressure and at high temperatures. For that, we have applied the quasi-harmonic Debye approximation. We start first by calculating a set of total energy as a function of the primitive cell volume (E–V) in the static approximation. Then, the obtained data are fit with a numerical EOS so as to obtain the structural parameters at pressure and temperature of zero, and to derive the macroscopic properties versus pressure and temperature using standard thermodynamic relations.

The diagrams that represent the volume unit-cell temperature at various pressures and lattice constant pressure

Table 2 Calculated energy band gap for orthorhombic and cubic phases using GGA-PBE, GGA-EV, GGA-WC, GGA-Sol and GGA + *U* approaches

Compounds	This work (FP-LAPW)			This work (PP-PW)			Exp	Others
	GGA-PBE	GGA-EV	GGA + *U*	GGA-PBE	GGA-Sol	GGA-WC		
$BaZrS_3$								
(*Pnma*)	1.051	1.424	1.063	1.202	1.109	1.117	1.8 [70] 1.8 [76]	1.02 [78] 1.82 [79] 1.7 [80] 2.34 [81] 2.25 [82]
(*Pm-3m*)	0.553	0.996	0.548	0.554	0.425	0.545	–	–
$CaZrS_3$								
(*Pnma*)	1.311	1.637	1.362	1.303	1.177	1.185	1.90 [70]	2.48 [78] 2.48 [82]
(*Pm-3m*)	0.446	0.899	0.469	0.424	0.288	0.325		
$SrZrS_3$								
(*Pnma*)	1.268	1.617	1.288	1.280	1.151	1.160	2.13 [70]	2.04 [76] 2.50 [79] 2.50 [82]
(*Pm-3m*)	0.492	0.975	0.492	0.492	0.383	0.400	–	–

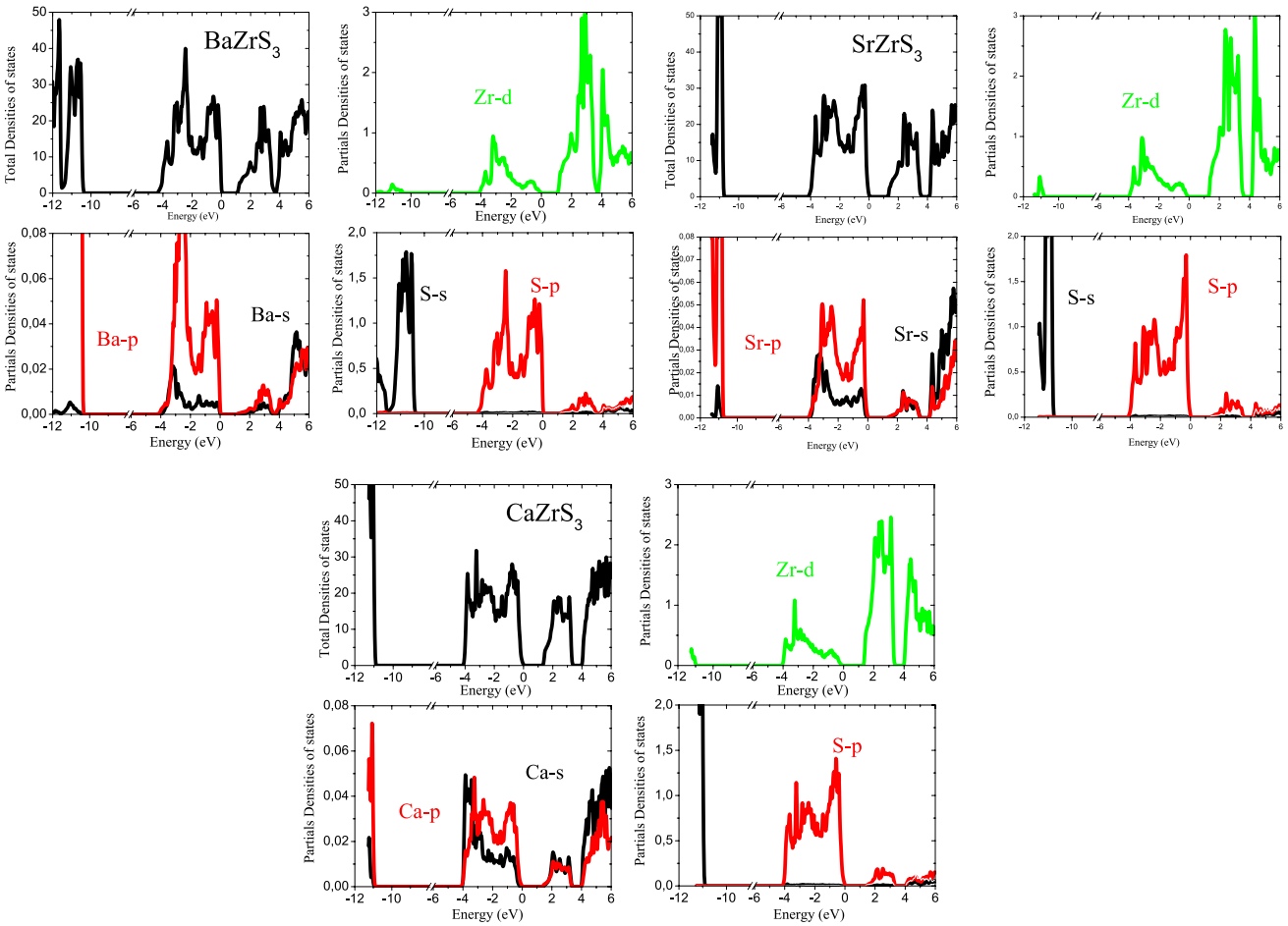

Fig. 5 Total and projected density of states of *Pbnm* structure using PBE-GGA method

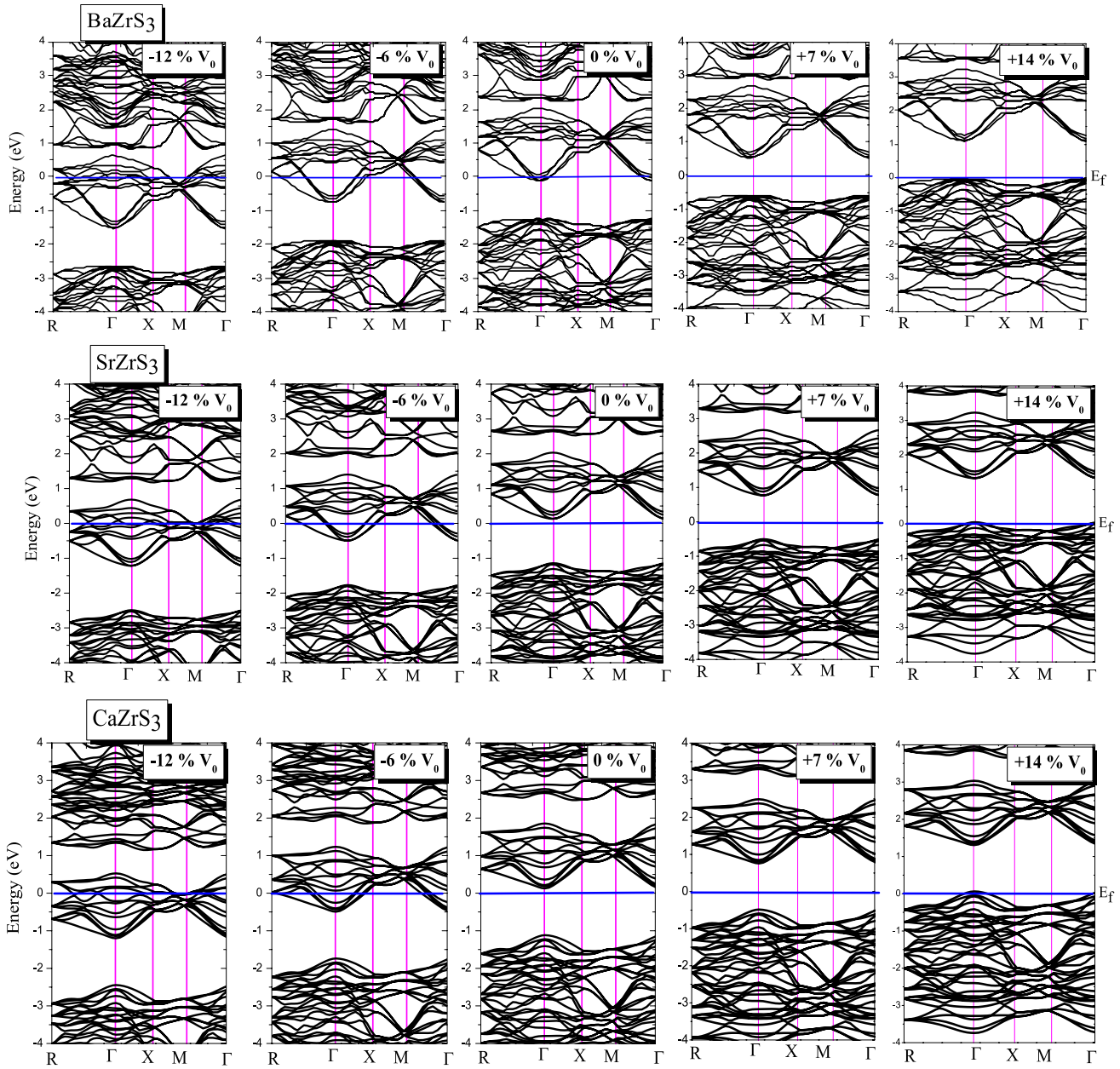

Fig. 6 Calculated band structure of *Pbnm* structure using PBE-GGA method: pressure effect

at different temperatures for all compounds being studied here are shown in Fig. 7. Note that for a given pressure, the lattice constant increases monotonically with rising temperature. Nevertheless, the rate of increase seems to be very moderate. On the other hand, for a given temperature, the lattice constant decreases with increasing pressure. In the present work, our calculated volumes for $BaZrS_3$, $SrZrS_3$ and $CaZrS_3$ compounds at zero pressure and room temperature are found to be 509.31, 480.13 and 453.47 $Å^3$, respectively.

The variation of the bulk modulus as a function of temperature at different pressures ranging from 0 to 30 GPa is plotted in Fig. 8. We observe that the bulk modulus varies almost linearly versus temperature for all pressures of interest. It decreases monotonically and very slowly with the rising temperature. Our calculations of the bulk modulus at a temperature of 300 K and zero pressure yielded values of 292.33, 308.86 and 329.16 GPa for $BaZrS_3$, $SrZrS_3$ and $CaZrS_3$ compounds, respectively.

The evolution of the heat capacity at a constant volume C_V as a function of temperature at various pressures ranging from 0 to 30 GPa is displayed in Fig. 9. Note that C_V increases with rising temperature. The behavior appears to be rapid at low temperatures but becomes slow at high temperatures. For temperatures less than 900 K, C_V

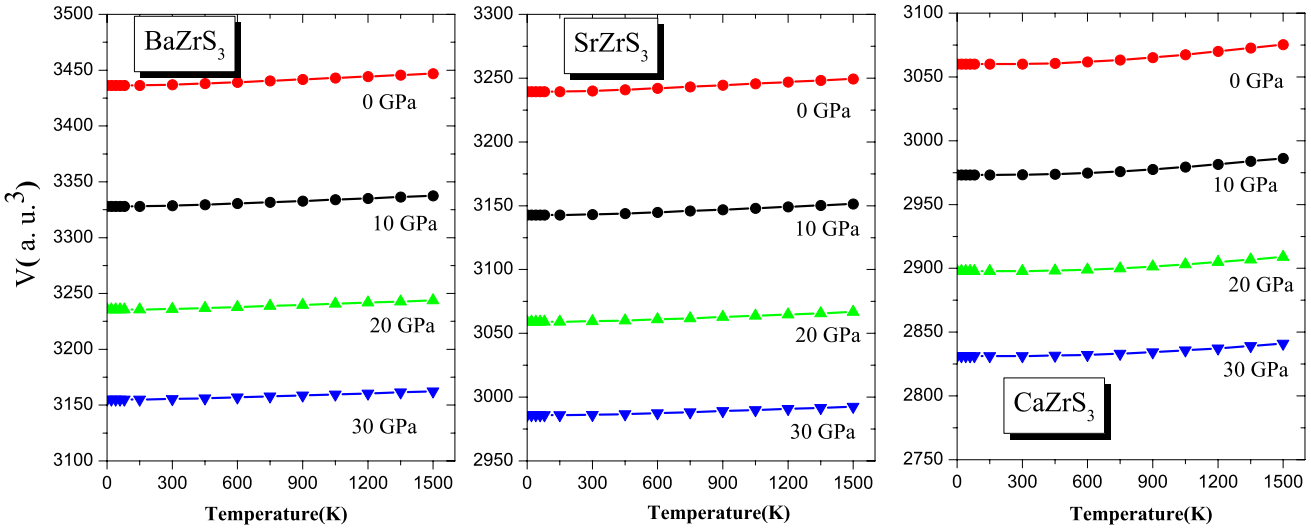

Fig. 7 Temperature dependence of the volume at various pressures for $XZrS_3$ compounds

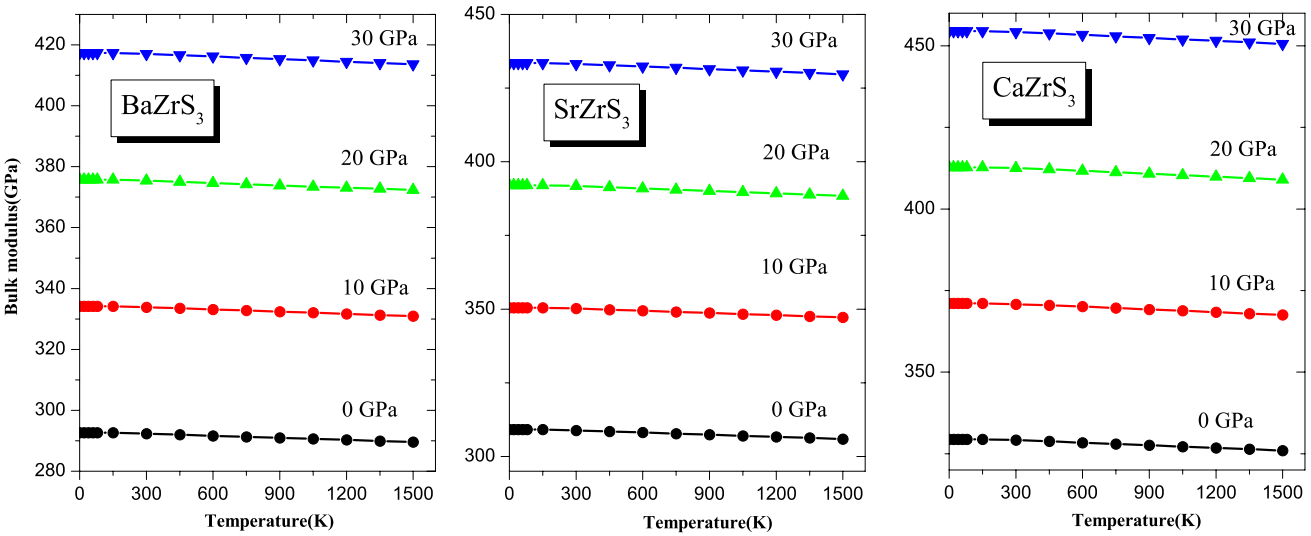

Fig. 8 Temperature dependence of the Bulk modulus *B* at various pressures for $XZrS_3$ compounds

depends on both temperature and pressure. At high temperatures, C_V approaches approximately 121.94, 120.92 and 120.17 J mol^{-1} K^{-1} for $BaZrS_3$, $SrZrS_3$ and $CaZrS_3$ compounds, respectively. The details in this change seem to depend on pressure. The behavior of C_V for all compounds of interest exhibits similar features in a wide range of pressures and temperatures. At zero pressure and a temperature of 300 K, our findings yielded values of C_V of about 81.98, 75.38 and 61.98 J mol^{-1} K^{-1} for $BaZrS_3$, $SrZrS_3$ and $CaZrS_3$ compounds, respectively. In order to reflect the temperature dependence of the volume, the Debye temperature is calculated using the quasi-harmonic Debye approximation. Our results are shown in Fig. 10. Note that the Debye temperature of all compounds in question increases with rising temperature. It is worth noting that the Debye temperature decreases with increasing the atomic number of X (X = Ba, Sr and Ca). The temperature dependence of the thermal expansion coefficient α of the (Ca, Sr, Ba)ZrS_3 compounds at various pressures is depicted in Fig. 11; it is clear that below 600 K, the thermal expansion coefficient increases rapidly, whereas at temperatures higher than 600 K, the α value initially remains constant and then increases linearly at high pressure. At zero pressure and T = 300 K, α takes the values of $0.16\times10^{-5}K^{-1}$, 0.13×10^{-5} K^{-1} and 0.17×10^{-5} K^{-1} for $CaZrS_3$, $SrZrS_3$ and $BaZrS_3$, respectively.

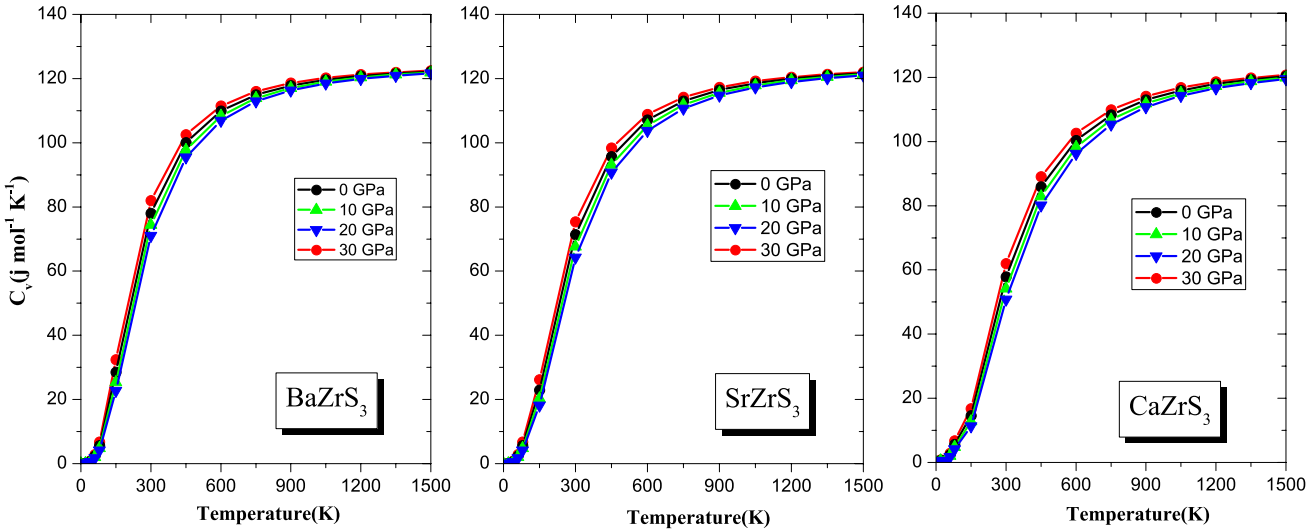

Fig. 9 Variation of the heat capacities Cv versus temperature at various pressures for $XZrS_3$ compounds

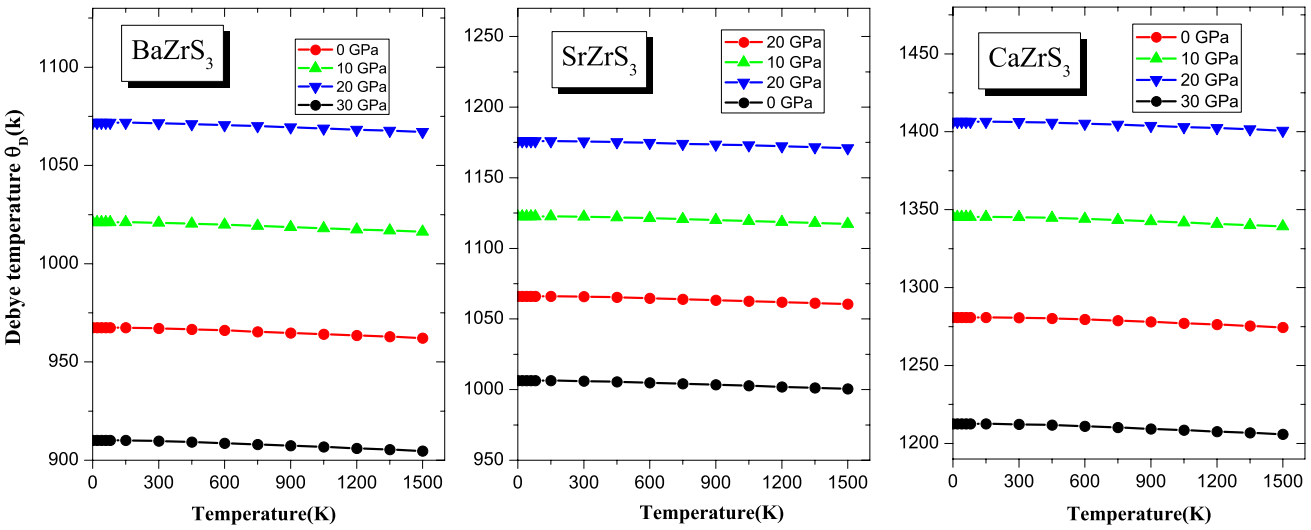

Fig. 10 Variation of the Debye temperature θ_D as function of temperature at various pressures for $XZrS_3$ compounds

4 Conclusion

In conclusion, the electronic and structural properties of cubic and orthorhombic $XZrS_3$(X = Ba, Sr, Ca) were investigated using both PP-PW and FP-LAPW methods. The computed lattice parameters, namely *a*, b and *c*, and the bulk modulus and its first pressure derivative were found to be in good accord with data available in the literature. Our results regarding the electronic band structures showed that the transition in the cubic phase occurs along R-Γ in the first Brillouin zone indicating thus that the material of interest is an indirect band-gap semiconductor in this phase. However, the transition in the orthorhombic phase was found to occur along Γ-Γ in the first Brillouin zone suggesting that the material of interest is a direct band-gap semiconductor in that phase. The semiconducting materials $XZrS_3$ of interest were found to be stable against volume change of 0 to + 14%. The thermal and pressure effects on the macroscopic

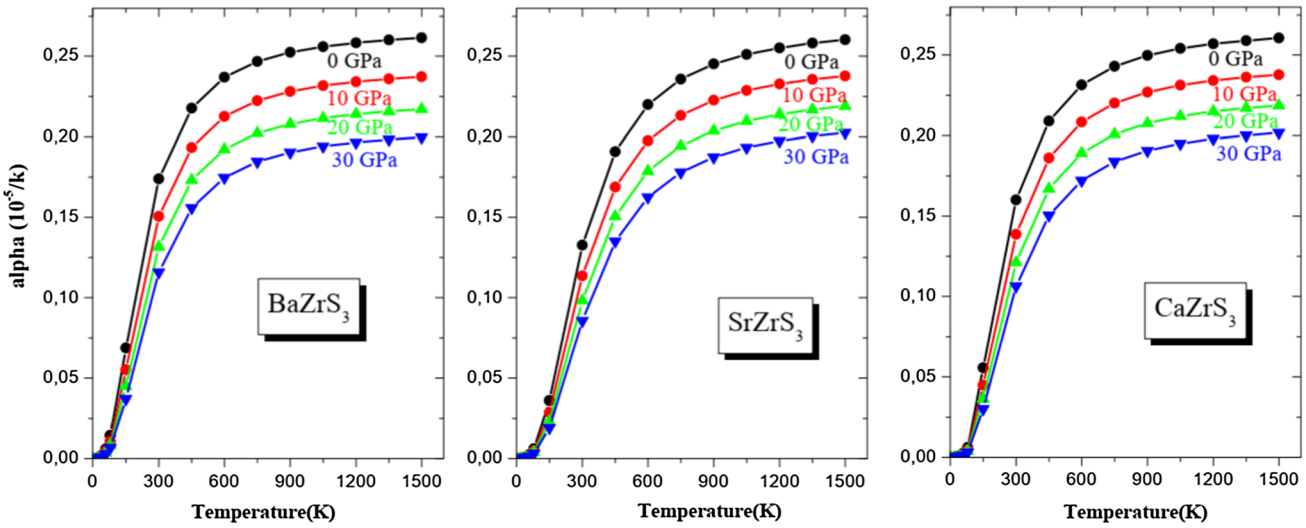

Fig. 11 Variation of the thermal expansion coefficient α of the XZrS3 compounds versus temperature at several pressures

properties of the compounds under study were predicted using the quasi-harmonic Debye model where the lattice vibrations were taken into consideration. The behavior of the lattice constant, bulk modulus, heat capacity, Debye temperature and thermal expansion coefficient as a function of both temperature and pressure was examined.

References

1. Soukiassian, A., Tian, W., Vaithyanathan, V., Haeni, J.H., Chen, L.Q., Xi, X.X., Schlom, D.G., Tenne, D.A., Sun, H.P., Pan, X.Q., Choi, K.J., Eom, C.B., Li, Y.L., Jia, Q.X., Constantin, C., Feenstra, R.M., Bernhagen, M., Reiche, P., Uecker, R.: Growth of nanoscale $BaTiO_3/SrTiO_3$ superlattices by molecular-beam epitaxy. J. Mater. Res. **23**, 1417–1432 (2008)
2. Jang, H.W., Baek, S.H., Ortiz, D., Folkman, C.M., Eom, C.B., Chu, Y.H., Shafer, P., Ramesh, R., Vaithyanathan, V., Schlom, D.G.: Epitaxial (001) BiFeO3 membranes with substantially reduced fatigue and leakage. Appl. Phys. Lett. **92**, 062910–062913 (2008)
3. Wolframand, T., Ellialtioglu, S.: Electronic and Optical Properties of d-Band Perovskites, pp. 280–303. Cambridge University Press, Cambridge (2006)
4. Wu, M., Fang, L., Liu, L., Li, G., Elouadi, B.: Dielectric and ferroelectric properties of $(1-x)BiFeO_{3-x}Bi_{0.5}Na_{0.5}TiO_3$. Solid Solution Ferroelectr. **478**(1), 18–25 (2015)
5. Chen, P., Podraza, N.J., Xu, X.S., Melville, A., Vlahos, E., Gopalan, V., Ramesh, R., Schlom, D.G., Musfeldt, J.L.: Optical properties of quasi-tetragonal thin films. Appl. Phys. Lett. **96**, 131907 (2010)
6. Chong, N.S., Suen, N.T., Chou, T.L., Tang, H.Y.: Electrocrystallization and characterization of polymorphic forms of barium metaplumbate. Cryst. Growth Des **8**(5), 1779–1782 (2008)
7. Christen, H.-M., Boatner, L.A., Budai, J.D., Chisholm, M.F., Gea, L.A., Norton, D.P., Gerber, C., Urbanik, M.: Semiconducting epitaxial films of metastable $SrRu_{0.5}Sn_{0.5}O_3$ grown by pulsed laser deposition. Appl. Phys. Lett. **70**, 2147 (1997)
8. Balachandran, U., Ma, B., Maiya, P.S., Mievillea, R.L., Duseka, J.T., Piccioloa, J.J., Guana, J., Dorrisa, S.E., Liub, M.: Development of mixed-conducting oxides for gas separation. Solid State Ion. **108**, 363–370 (1998)
9. Kawada, T., Sase, M., Kudo, M., Yashiro, K., Sato, K., Mizusaki, J., Sakai, N., Horita, T., Yamaji, K., Yokokawa, H.: Microscopic observation of oxygen reaction pathway on high temperature electrode materials. Solid State Ion. **177**, 3081–3086 (2006)
10. Hrovat, M., Katsarakis, N., Reichmann, K., Bernik, S., Kuščer, D., Holc, J.: Characterisation of $LaNi_{1-x}Co_xO_3$ as a possible SOFC cathode material. Solid State Ion. **83**(1–2), 99–105 (1996)
11. Joshi, U.A., Jang, J.S., Borse, P.H., Lee, J.S.: Microwave synthesis of single-crystalline perovskite $BiFeO_3$ nanocubes for photoelectrode and photocatalytic applications. Appl. Phys. Lett. **92**, 242106 (2008)
12. Ramasamy, P., Lim, D.-H., Kim, B., Lee, S.-H., Lee, M.-S., Lee, J.-S.: All- inorganic cesium lead halide perovskite nanocrystals for photodetector applications. Chem. Commun. **52**, 2067–2070 (2016)
13. Slavney, A.H., Hu, T., Lindenberg, A.M., Karunadasa, H.I.: A bismuth-halide double perovskite with long carrier recombination lifetime for photovoltaic applications. J. Am. Chem. Soc. **138**(7), 2138–2141 (2016)
14. Huang, K., Feng, M., Goodenough, J.B.: Sol–gel synthesis of a new oxide-ion conductor sr- and mg-doped LaGaO3 perovskite. J. Am. Ceram. Soc. **79**, 1100–1104 (1996)
15. Iwahara, H., Esaka, T., Uchida, H., Maeda, N.: Proton conduction in sintered oxides and its application to steam electrolysis for hydrogen production. Solid State Ion. **3–4**, 359–363 (1981)
16. Uchida, H., Maeda, N., Iwahara, H.: Relation between proton and hole conduction in $SrCeO_3$-based solid electrolytes under water-containing atmospheres at high temperatures. Solid State Ion. **11**(2), 117–124 (1983)
17. Iwahara, H., Uchida, H., Ono, K., Ogaki, K.: Proton conduction in sintered oxides based on $BaCeO_3$. J. Electrochem. Soc. **135**(2), 529–533 (1988)

18. Dimos, D., Mueller, C.: Perovskite thin films for high-frequency capacitor applications. Annu. Rev. Mater. Res. **28**, 397–419 (1998)
19. Shaw, T., Trolier-McKinstry, S., McIntyre, P.: The properties of ferroelectric films at small dimensions. Annu. Rev. Mater. Sci. **30**, 263–298 (2000)
20. Higuchi, Y., Tamura, H.: Recent progress on the dielectric properties of dielectric resonator materials with their applications from microwave to optical frequencies. J. Eur. Ceram. Soc. **23**(14), 2683–2688 (2003)
21. Jonker, G.H.: Influence of grain boundary on magnetoresistance in hole doped manganites $La_{0.7}Ca_{0.3}MnO_3$, $La_{0.7}Sr_{0.3}MnO_3$ and $(La_{0.75}Y_{0.25})_{0.7}Sr_{0.3}MnO_3$. Physica **22**(8), 707–722 (1956)
22. De Teresa, J., Ibarra, M., Algarabel, P., Ritter, C., Marquina, C., Blasco, J., et al.: Evidence for magnetic polarons in the magnetoresistive perovskites. Nature **386**(6622), 256–259 (1997)
23. Moritomo, Y., Asamitsu, A., Kuwahara, H., Tokura, Y.: Giant magnetoresistance of manganese oxides with a layered perovskite structure. Nature **380**(6570), 141–144 (1996)
24. Moret, M.P., Devillers, M., Worhoff, K., Larsen, P.: Optical properties of $PbTiO_3$, $PbZr_xTi_{1-x}O_3$, and $PbZrO_3$ films deposited by metalorganic chemical vapor on $SrTiO_3$. J. Appl. Phys. **92**(1), 468–474 (2002)
25. Jona, F., Shirane, G., Pepinsky, R.: Optical study of $PbZrO_3$ and $NaNbO_3$ single crystals. Phys. Rev. **97**(6), 1584–1590 (1955)
26. Weber, M.J., Bass, M., Demars, G.: Laser action and spectroscopic properties of Er^{3+} in $YAlO_3$. J. Appl. Phys. **42**(1), 301 (1971)
27. Rao, K., Yoon, K.: Review of electrooptic and ferroelectric properties of barium sodium niobate single crystals. J. Mater. Sci. **38**(3), 391–400 (2003)
28. Ihringer, J., Maichle, J., Prandl, W., Hewat, A., Wroblewski, T.: Crystal structure of the ceramic superconductor $BaPb_{0.75}Bi_{0.25}O_3$. Z. Phys. B Condens. Matter **82**(2), 171–176 (1991)
29. Cava, R.J., Batlogg, B., Krajewski, J.J., Farrow, R., Rupp, L.W., White, A.E., et al.: Superconductivity near 30 K without copper: the $Ba_{0.6}K_{0.4}BiO_3$ perovskite. Nature **332**(6167), 814–816 (1988)
30. Sampathkumar, T., Srinivasan, S., Nagarajan, T., Balachandran, U.: Properties of $YBa_2Cu_3O_7$-δ-$BaBiO_3$ composite superconductors. Appl. Superconduct. **2**(1), 29–34 (1994)
31. Frederikse, H.P.R., Thurber, W.R., Hosler, W.R.: Electronic transport in strontium titanate. Phys. Rev. **134**, 442 (1964)
32. Samantaray, C.B., Sim, H., Hwang, H.: Electronic structure and optical properties of barium strontium titanate ($Ba_xSr_{1-x}TiO_3$) using first-principles method. Phys. B Condens. Matter **351**(1–2), 158–162 (2004)
33. Bednorz, J.G., Müller, K.A.: $Sr_{1-x}Ca_xTiO_3$: an XY quantum ferroelectric with transition to randomness. Phys. Rev. Lett. **52**, 2289 (1984)
34. Berri, S., Maouche, D., Ibrir, M., Bakri, B.: Electronic structure and magnetic properties of the perovskite cerium manganese oxide from ab initio calculations. Mater. Sci. Semicond. Process. **26**, 199–204 (2014)
35. Raza urrehman Hashmi, M., Zafar, M., Shakil, M., Sattar, A., Ahmed, S., Ahmad, S.A.: First-principles calculation of the structural, electronic, and magnetic properties of cubic perovskite RbXF3 (X = Mn, V Co, Fe). Chin. Phys. B **25**(11), 117401 (2016)
36. Khandy, S.A., Gupta, D.C.: Structural, elastic and magneto-electronic properties of half-metallic $BaNpO_3$ perovskite. Mater. Chem. Phys. **198**, 380–385 (2017)
37. Berri, S.: Search for new half-metallic ferromagnets in quaternary diamond-like compounds I-II2–III–VI4 and I2–II–IV–VI4 (I = Cu; II = Mn, Fe, Co; III = In; IV = Ge, Sn; VI = S, Se, Te). J. Superconduct. Novel Magn. **31**(6), 1941–1947 (2018)
38. Berri, S.: Half-metallic ferromagnetism in Li6VCl8, Li6MnCl8, Li6CoCl8 and Li6FeCl8 from first principles. J. Superconduct. Novel Magn. **29**(9), 2381–2386 (2016)
39. Berri, S., Kouriche, A., Maouche, D., Zerarga, F., Attallah, M.: Ab initio study of electronic structure and magnetic properties in ferromagnetic Sr_{1-x}(Mn, Cr)xO alloys. Mater. Sci. Semiconduct. Process. **38**, 101–106 (2015)
40. Berber, M., Doumi, B., Mokaddem, A., Mogulkoc, Y., Sayede, A., Tadjer, A.: Investigation of electronic structure and half-metallic ferromagnetic behavior with large half-metallic gap in $Sr_{1-x}V_xO$. J. Comput. Electron. **13**, 542–547 (2017)
41. Berri, S.: First-principles study on half-metallic properties of the Sr2GdReO6 double perovskite. J. Magn. Magn. Mater. **385**, 124–128 (2015)
42. Wang, X., Khachai, H., Khenata, R., Yuan, H., Wang, L., Wang, W., Bouhemadou, A., Hao, L., Dai, X., Guo, R., Liu, G., Cheng, Z.: Structural, electronic, magnetic, half-metallic, mechanical, and thermodynamic properties of the quaternary Heusler compound FeCrRuSi: a first-principles study. Sci. Rep. **7**(1), 16183 (2017)
43. Brehm, J.A., Bennett, J.W., Schoenberg, M.R., Rappe, I., Grinberg, A.M.: The structural diversity of ABS_3 compounds with d^0 electronic configuration for the *B*-cation. J. Chem. Phys. **140**, 224703 (2014)
44. Körbel, S.K.X., Marques, M.A.L., Botti, S.: Stability and electronic properties of new inorganic perovskites from high-throughput ab initio calculations. J. Mater. Chem. C **4**, 3157–3167 (2016)
45. Kuhar, K., Crovetto, A., Pandey, M., Thygesen, K., Seger, B., Vesborg, P.C.K., Hansen, O., Chorkendorff, I., Jacobsen, K.W.: Sulfide perovskites for solar energy conversion applications: computational screening and synthesis of the selected compound $LaYS_3$. Energy Environ. Sci. **10**, 2579 (2017)
46. Ju, M.-G., Dai, J., Ma, L., Zeng, X.C.: Perovskite chalcogenides with optimal bandgap and desired optical absorption for photovoltaic devices. Adv. Energy Mater. **7**, 1700216 (2017)
47. Nijamudheen, A., Akimov, A.V.: Criticality of symmetry in rational design of chalcogenide perovskites. J. Phys. Chem. Lett. **9**, 248–257 (2018)
48. Sun, Y.-Y., Agiorgousis, M.L., Zhang, P., Zhang, S.: Chalcogenide perovskites for photovoltaics. Nano Lett. **15**, 581–585 (2015)
49. Hong, F., Saparov, B., Meng, W., Xiao, Z., Mitzi, D.B., Yan, Y.: Viability of lead-free perovskites with mixed chalcogen and halogen anions for photovoltaic applications. J. Phys. Chem. C **120**(12), 6435–6441 (2016)
50. Kuhar, K., Pandey, M., Thygesen, K.S., Jacobsen, K.W.: High-throughput computational assessment of previously synthesized semiconductors for photovoltaic and photoelectrochemical devices. ACS Energy Lett. **3**, 436–446 (2018)
51. Enkovaara, J., Rostgaard, C., Mortensen, J.J., Chen, J., Dułak, M., Ferrighi, L., Gavnholt, J., Glinsvad, C., Haikola, V., Hansen, H.A., et al.: Electronic structure calculations with GPAW: a real-space implementation of the projector augmented-wave method. J. Phys. Condens. Matter **22**, 253202 (2010)
52. Lelieveld, R., Ijdo, D.J.W.: Sulphides with the $GdFeO_3$ structure. Acta Cryst. B **36**, 2223–2226 (1980)
53. Blaha, P., Schwarz, K., Madsen, G.K.H., Kvasnicka, D., Luitz, J.: WIEN2K, An Augmented Plane Wave +Local Orbitals Program for Calculating Crystal Properties. Karlheinz Schwarz, Technische Universität, Wien (2001). ISBN 3-9501031-1-2
54. Perdew, J.P., Burke, S., Ernzerhof, M.: Generalized gradient approximation made simple. Phys. Rev. Lett. **77**, 3865 (1996)
55. Engel, E., Vosko, S.H.: Generalized gradient approximation for the relativistic exchange-only energy functional. Phys. Rev. B **47**, 1316 (1993)

56. Loschen, C., Carrasco, J., Neyman, K.M., Illas, F.: First-principles LDA + U and GGA + U study of cerium oxides: dependence on the effective U parameter. Phys. Rev. B **75**, 035115 (2007)
57. Vanderbilt, D.: Soft self-consistent pseudopotentials in a generalized eigenvalue formalism. Phys. Rev. B **41**, 7892 (1990)
58. Perdew, J.P., Ruzsinszky, A., Csonka, G.I., Vydrov, O.A., Scuseria, G.E., Constantin, L.A., Zhou, X., Burke, K.: Restoring the density-gradient expansion for exchange in solids and surfaces. Phys. Rev. Lett. **100**, 136406 (2008)
59. Wu, Z., Cohen, R.E.: More accurate generalized gradient approximation for solids. Phys. Rev. B **73**, 235116 (2006)
60. Segall, M.D., Lindan, P.J.D., Probert, M.J., Pickard, C.J., Hasnip, P.J., Clark, S.J., Payne, M.C.: First-principles simulation: ideas, illustrations and the CASTEP code. J. Phys. Condens. Matter **14**, 2717 (2002)
61. Fischer, T.H., Almlof, J.: General methods for geometry and wave function optimization. J. Phys. Chem. **96**, 9768 (1992)
62. Blanco, M.A., Francisco, E., Luaña, V.: GIBBS: isothermal-isobaric thermodynamics of solids from energy curves using a quasi-harmonic Debye model. Comput. Phys. Commun. **158**, 7 (2004)
63. Blanco, A., Martín Pendàs, A., Francisco, E., Recio, J.M., Franco, R.: Thermodynamical properties of solids from microscopic theory: applications to MgF_2 and Al_2O_3. J. Mol. Struct. Theochem. **368**, 45 (1996)
64. Flãrez, M., Recio, J.M., Francisco, E., Blanco, M.A., Martìn Pendás, A.: First-principles study of the rocksalt–cesium chloride relative phase stability in alkali halides. Phys. Rev. B **66**, 144112 (2002)
65. Francisco, E., Recio, J.M., Blanco, M.A., Martín Pendás, A., Costales, A.: Quantum-mechanical study of thermodynamic and bonding properties of MgF_2. J. Phys. Chem. A **102**, 1595–1601 (1998)
66. Francisco, E., Blanco, M.A., Sanjurjo, G.: Atomistic simulation of SrF2 polymorphs. Phys. Rev. B **63**, 94107 (2001)
67. Poirier, J.P.: Introduction to the Physics of the Earth's Interior, p. 39. Cambridge University Press, Oxford (2000)
68. Hill, R.: The elastic behaviour of a crystalline aggregate. Proc. Phys. Soc. Lond. A **65**, 49 (1952)
69. Murnaghan, F.D.: The compressibility of media under extreme pressures. Proc. Natl. Acad. Sci. USA **30**, 244 (1944)
70. Perera, S., Hui, H., Zhao, C., Xue, H., Sun, F., Gross, C.D.N., Milleville, C., Xu, X., Watson, D.F., Weinstein, B., Sun, Y.-Y., Zhang, S., Zeng, H.: Chalcogenide perovskites—an emerging class of ionic semiconductors. Nano Energy **22**, 129–135 (2016)
71. W. Pies and A. Weiss. Landolt-Börnstein. Numerical data and functional relationships in science and technology. Group III. Crystal and solid state physics. Crystal structure data of inorganic compounds. Acta Crystallogr. Sect. A Cryst. Phys. Differ. Theor. Gen. Crystallogr. 271–272 (1975)
72. Swarnkar, A., Mir, W.J., Chakraborty, R., Jagadeeswararao, M., Sheikh, T., Nag, A.: Are chalcogenide perovskites an emerging class of semiconductors for optoelectronic properties and solar cell? Chem. Mater **31**(3), 565–575 (2019)
73. Evarestov, R.A.: Hybrid density functional theory LCAO calculations on phonons in $Ba(Ti, Zr, Hf)_3$. Phys. Rev. B Condens. Matter Mater. Phys. **83**, 014105 (2011)
74. Eglitis, R.I.: Ab initio calculations of the atomic and electronic structure of $BaZrO_3$ (111) surfaces. Solid State Ion. **230**, 43–47 (2013)
75. Bjørheim, T.S., Arrigoni, M., Gryaznov, D., Kotomin, E., Maier, J.: Thermodynamic properties of neutral and charged oxygen vacancies in $BaZrO_3$ based on first principles phonon calculations. Phys. Chem. Chem. Phys. **17**, 20765 (2015)
76. Bilić, A., Gale, J.D.: Ground state structure of $BaZrO_3$: a comparative first-principles study. Phys. Rev. B Condens. Matter **79**, 174107 (2009)
77. Meng, W., Saparov, B., Hong, F., Wang, J., Mitzi, D.B., Yan, Y.: Alloying and defect control within chalcogenide perovskites for optimized photovoltaic application. Chem. Mater. **28**(3), 821–829 (2016)
78. Polfus, J.M., Norby, T., Bredesen, R.: Protons in oxysulfides, oxysulfates, and sulfides: a first-principles study of La_2O_2S, $La_2O_2SO_4$, $SrZrS_3$, and $BaZrS_3$. J. Phys. Chem. C **119**, 23875–23882 (2015)
79. Wyckoff, R.: Inorganic Compounds RXn, RnMX2, RnMX3. Crystal Structures, vol. 2. R.E. Krieger Pub. Co., Malabar (1982)
80. Lopez-Garcia, A., Alonso, R., Falabella, M., Echeverría, G.: The effect of oxygen vacancies in $Ca_{1-x}Sr_xHfO_3$. Ferroelectrics **396**(1), 37–48 (2010)
81. Brik, M., Ma, C.-G., Krasnenko, V.: First-principles calculations of the structural and electronic properties of the cubic CaZrO3 (001) surfaces. Surf. Sci. **608**, 146–153 (2013)
82. Moreira, R.L., Dias, A.: Comment on "Prediction of lattice constant in cubic perovskites". J. Phys. Chem. Solids **68**, 1617 (2007)
83. Sandeep, D.P., Rai, A., Shankar, M.P., Ghimire, R., Khenata, S., Omran, B., Syrotyuk, S.V., Thapa, R.K.: Investigation of the structural, electronic and optical properties of the cubic $RbMF_3$ perovskites (M = Be, Mg, Ca, Sr and Ba) using modified Becke-Johnson exchange potential. Mater. Chem. Phys. **192**, 282–290 (2017)